ATM and ATR Substrate Analysis Reveals Extensive Protein Networks Responsive to DNA Damage

Shuhei Matsuoka, *et al.*

Science **316**, 1160 (2007);
DOI: 10.1126/science.1140321

ATM and ATR Substrate Analysis Reveals Extensive Protein Networks Responsive to DNA Damage

Shuhei Matsuoka,[1] Bryan A. Ballif,[2]* Agata Smogorzewska,[1,3]† E. Robert McDonald III,[1]† Kristen E. Hurov,[1]† Ji Luo,[1]† Corey E. Bakalarski,[2] Zhenming Zhao,[1] Nicole Solimini,[1] Yaniv Lerenthal,[4] Yosef Shiloh,[4] Steven P. Gygi,[2]‡ Stephen J. Elledge[1]‡

Cellular responses to DNA damage are mediated by a number of protein kinases, including ATM (ataxia telangiectasia mutated) and ATR (ATM and Rad3-related). The outlines of the signal transduction portion of this pathway are known, but little is known about the physiological scope of the DNA damage response (DDR). We performed a large-scale proteomic analysis of proteins phosphorylated in response to DNA damage on consensus sites recognized by ATM and ATR and identified more than 900 regulated phosphorylation sites encompassing over 700 proteins. Functional analysis of a subset of this data set indicated that this list is highly enriched for proteins involved in the DDR. This set of proteins is highly interconnected, and we identified a large number of protein modules and networks not previously linked to the DDR. This database paints a much broader landscape for the DDR than was previously appreciated and opens new avenues of investigation into the responses to DNA damage in mammals.

Genotoxic stress is a life-threatening event for organisms as it alters the content and organization of the genetic material. Organisms have developed multiple mechanisms to ameliorate the damage caused by genotoxic stress, including specialized DNA repair processes such as base excision repair, nucleotide excision repair, and nonhomologous end-joining that recognize and repair specific lesions in stereotypical ways. There is also a global signaling network called the DNA damage response (DDR) that senses different types of damage and coordinates a response that includes activation of transcription, cell cycle control, apoptosis, senescence, and DNA repair processes (*1*). This coordination is critical for cell survival, in particular when DNA replication is perturbed.

At the core of the DNA damage signaling apparatus are a pair of related protein kinases, ATM (ataxia telangiectasia mutated) and ATR (ATM and Rad3-related), which are activated by DNA damage. ATM with its regulator the MRN (Mre11-Rad50-NBS1) complex senses double-strand breaks (DSBs) (*2*). ATR with its regulator ATRIP (ATR-interacting protein) senses single-strand DNA (ssDNA) generated by processing of DSBs, as well as ssDNA present at stalled replication forks. Both kinases then phosphorylate proteins to initiate a signaling cascade that includes many common substrates including Chk1 and Chk2 (checkpoint kinases) that initiate a secondary wave of phosphorylation events to extend signaling. About 25 ATM and ATR substrates have been identified (*3*), many as candidates based on known roles in damage signaling.

A key to understanding any kinase network is the identification of the in vivo substrates. However, unbiased identification of kinase substrates is a difficult endeavor. Various technologies have emerged to identify phosphoproteins and kinase substrates (*4*, *5*), but few give in vivo confirmation or the sites of phosphorylation. Protein immunoprecipitation (IP) with antibodies to phosphotyrosine has been used to identify tyrosine kinase substrates (*6*). A newer method uses peptide IP with phosphotyrosine antibodies and mass spectrometry (MS) to identify substrates of tyrosine kinases (*7*). ATM and ATR share substrate specificity, recognizing Ser-Gln (SQ) and Thr-Gln (TQ) motifs (*8*, *9*), and antibodies to phospho-SQ or phospho-TQ sites have enabled identification of a few ATM substrates by protein IP (*10*, *11*). We have combined antibodies to phospho-SQ or phospho-TQ sites, together with peptide IP and SILAC (stable isotope labeling with amino acids in cell culture) (*12*), to identify proteins regulated in response to DNA damage. We discovered a vast network of over 700 human and mouse proteins phosphorylated in response to DNA damage that

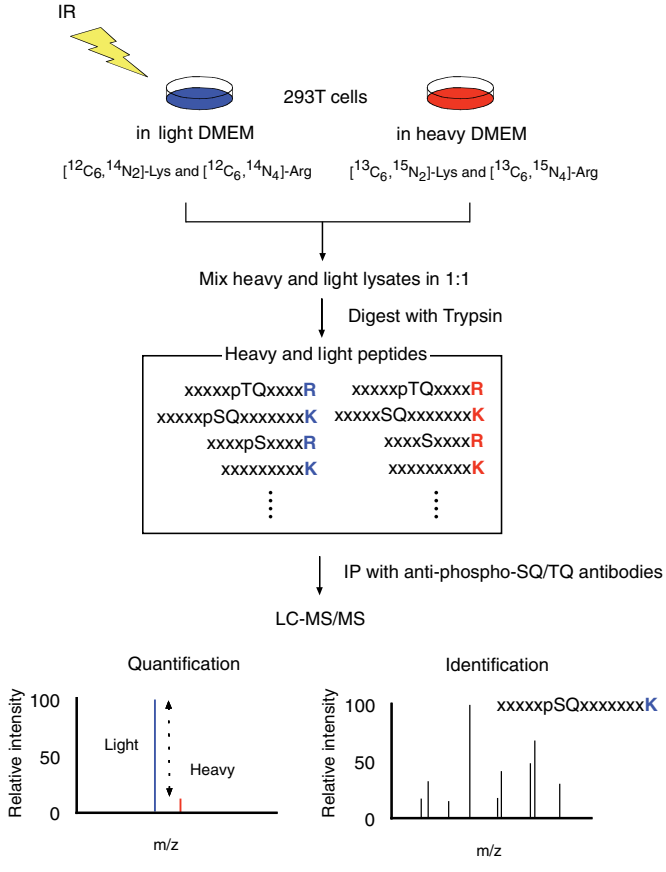

Fig. 1. Schematic for identification of DNA damage–regulated SQ and TQ sites. 293T cells were grown in heavy and light media, and cells in light medium were irradiated with 10 Gy of IR. Heavy and light cell lysates were combined, and peptides were immunoprecipitated with antibodies to phospho-SQ or phospho-TQ and applied to LC-MS/MS. Quantification of phosphorylation on each peptide was achieved by measuring the relative intensity of light and heavy peptides in the MS spectra, which are spaced by 8 daltons for peptides with Lys (K) or by 10 daltons for ones with Arg (R). Each phosphopeptide sequence was obtained from the MS/MS spectra.

[1]Department of Genetics and Center for Genetics and Genomics, Brigham and Women's Hospital, Howard Hughes Medical Institute, Harvard Medical School, Boston, MA 02115, USA. [2]Department of Cell Biology and Taplin Biological Mass Spectrometry Facility, Harvard Medical School, Boston, MA 02115, USA. [3]Department of Pathology, Massachusetts General Hospital, Boston, MA 02214, USA. [4]Department of Human Molecular Genetics and Biochemistry, Sackler School of Medicine, Tel Aviv University, Tel Aviv 69978, Israel.

*Present address: Department of Biology, University of Vermont, Burlington, VT 05405, USA.
†These authors contributed equally to this work.
‡To whom correspondence should be addressed. E-mail: selledge@genetics.med.harvard.edu, steven_gygi@hms.harvard.edu

represents many pathways not previously implicated in the response to DNA damage.

Results

Peptide IP and SILAC. We grew two populations of human embryonic kidney 293T cells in equivalent DMEM (Dulbecco's modified Eagle medium) except that one contained heavy [$^{13}C_6$, $^{15}N_4$]-Arg and [$^{13}C_6$, $^{15}N_2$]-Lys and the other contained light Arg and Lys (Fig. 1). Both cell types grew and responded to ionizing radiation (IR) normally (fig. S1). 293T cells grown in light medium were irradiated with 10 Gy of IR and collected 1 hour after irradiation. Heavy and light lysates were combined (1:1 ratio) and digested with trypsin, then 60 peptide IPs with 68 antibodies to phospho-SQ or phospho-TQ were performed. Bound peptides were applied to liquid chromatography–tandem MS (LC-MS/MS), and the abundance of each phosphopeptide was quantified by measuring the relative intensity of light and heavy peptides in the high-accuracy MS spectra. After quantification of SILAC phosphopeptide pairs, 905 phosphorylation sites on 700 proteins showed an increase in phosphorylation of more than fourfold after DNA damage by IR (table S1). A more limited analysis on mouse NIH3T3 cells identified 95 phosphorylation sites on 86 proteins. Of these, 55 sites were found on 47 mouse proteins whose human homologs were among the 700 human substrates (table S2).

Of the 68 antibodies used, 28 were against phosphorylation sites known to be phosphorylated after DNA damage, and 17 of these were recovered as sites regulated by DNA damage. Several new phosphorylation sites were identified among these targets: three sites each on ATM (T^{86}, S^{367}, and T^{373}), BRCA1 (breast cancer 1, early onset) (S^{1239}, S^{1330}, and T^{1720}), SMC1 (structural maintenance of chromosomes) (S^{358}, S^{360}, and S^{951}), TopBP1 (topoisomerase-binding protein 1) (S^{214}, T^{975}, and S^{1051}), and KAP1 (KRAB domain–associated protein 1) (S^{440}, S^{501}, and S^{824}) and four sites on FANCD2 (Fanconi anemia D2) (S^{178}, T^{596}, S^{717}, and S^{1418}). During the course of this study, some of these were shown to be phosphorylated in vivo after DNA damage (*11*, *13*, *14*). Altogether, we identified 55 regulated phosphorylation sites on the 31 candidate ATM and ATR substrates previously implicated in DNA damage signaling or repair (table S3).

Validation. We confirmed the phosphorylation status for a subset of the candidate substrate proteins by IP and Western blotting. MDC1 (mediator of DNA damage checkpoint 1), 53BP1 (p53-binding protein 1), Orc3 (origin recognition complex subunit 3), and an uncharacterized Zn-finger protein, ZCCHC8, identified with antibodies to phospho-BRCA1 S^{1423} were immunoprecipitated with antibodies to each protein before and after 10 Gy of IR and subjected to Western blotting with antibodies to phospho-BRCA1 S^{1423}. All three were phosphorylated after IR. Although no antibodies to Orc3 for IP were available, we were able to immunoprecipitate Orc3 with antibodies to Orc2 because the two proteins associate (*15*). Thus, Orc3 phosphorylation after IR was confirmed (Fig. 2A).

Sequences around sites identified with antibodies to phospho-BRCA1 S^{1423} are very similar to sequences around BRCA1 S^{1423} (Fig. 2A). We examined the distribution of amino acid residues surrounding the phosphorylation site among the phosphopeptides identified by individual peptide IPs (fig. S2). Most antibodies used recognize one or two amino acids at −1 or +2 position, in addition to the phospho-SQ or phospho-TQ. Normally, linear epitopes are thought to comprise five to seven amino acids. The presence of the phosphate on the epitope may reduce the number of additional contacts needed to form an immunogenic epitope. We also determined the distribution of amino acid residues surrounding the DNA damage–regulated phospho-SQ or -TQ sites on the 700 candidate ATM and ATR substrates. Enrichment of E (Glu) and S around the SQ or TQ sites was observed (Fig. 2B). This is consistent with the notion that E or D (Asp) is often found around SQ or TQ sequence phosphorylated by ATM or ATR in vitro (*8*).

Of the 11 proteins whose phosphorylation after IR was confirmed (Fig. 2A and fig. S3), we

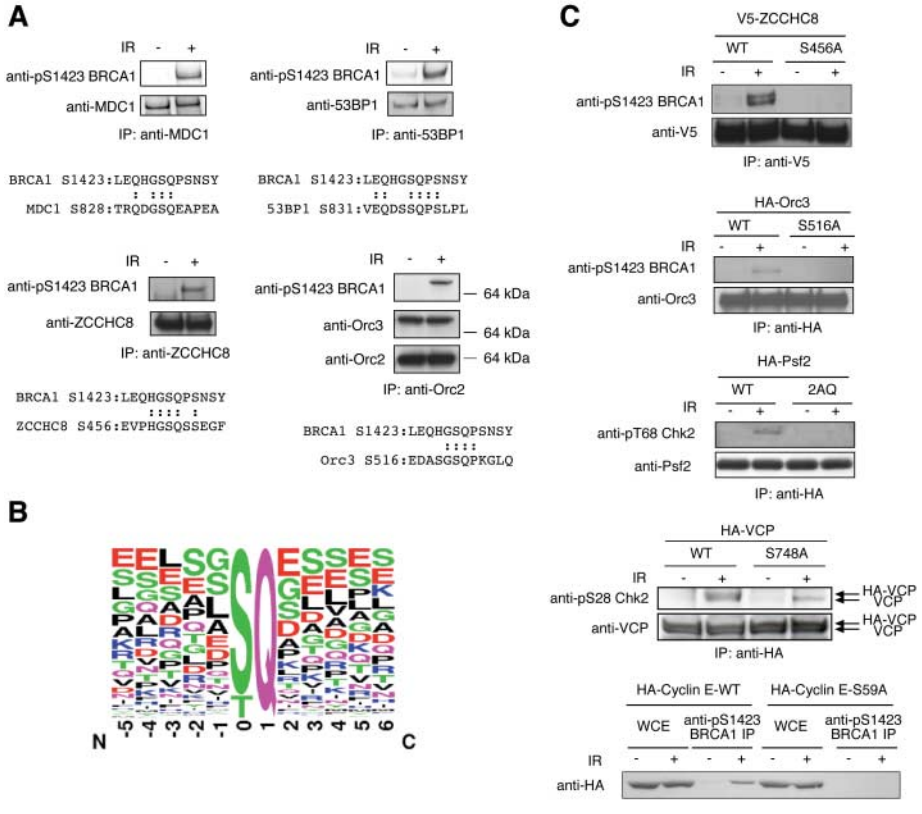

Fig. 2. Validation of protein phosphorylation. (**A**) MDC1, 53BP1, and ZCCHC8 were immunoprecipitated with antibodies against each protein from 293T cells before (-IR) and after (+IR) 10 Gy of IR, and precipitated proteins were subjected to Western blotting with antibodies to phospho-BRCA1 S^{1423}. The same blots were reprobed with antibodies to MDC1, 53BP1, or ZCCHC8. Orc3 was coimmunoprecipitated with antibodies to Orc2, and precipitated proteins were subjected to Western blotting with antibodies to phospho-BRCA1 S^{1423}. The same blot was reprobed with antibodies to Orc3 and Orc2. Sequences around the identified site on each protein were aligned with those around BRCA1 S^{1423}. (**B**) Distribution of amino acid residues (*30*) surrounding the phospho-SQ or -TQ sites on the candidate ATM and ATR substrates that were regulated by DNA damage. Sequence analysis was done with MOTIF-X software (*31*). (**C**) HA-tagged wild-type VCP, Orc3, or Psf2 (WT) or AQ mutant of each protein [VCP S748A, Orc3 S516A, and Psf2 T180A/S182A (2AQ)] was expressed in U2OS cells, and V5-tagged ZCCHC8 wild-type (WT) or AQ mutant (S456A) was expressed in 293T cells. Wild-type and AQ mutant proteins were immunoprecipitated with antibodies to HA or V5 from cells before (-IR) and after 10 Gy of IR (+IR) and probed with the indicated antibodies to phosphorylated sites. The same blots were reprobed with antibodies to each protein or anti-V5. Endogenous VCP (VCP) was coimmunoprecipitated with HA-tagged VCP (HA-VCP) by IP with antibodies to HA because VCP forms a homo hexamer (*32*). HA-tagged wild-type cyclin E (WT) or AQ mutant (S59A) was expressed in U2OS cells, and proteins immunoprecipitated with antibodies to phospho-BRCA1 S^{1423} from cells before (-IR) and after 10 Gy of IR (+IR) and whole-cell extracts (WCE) were subjected to Western blotting with antibodies to HA.

further validated 5 by mutating the identified sites. Substitution of AQ for the identified SQ or TQ site was introduced by site-direct mutagenesis into VCP (valosine-containing protein), Orc3, Psf2 (partner of SLD5), ZCCHC8, and cyclin E. In all five cases, phosphorylation was observed on wild-type proteins but not on AQ mutants (Fig. 2C), indicating that the antibodies were recognizing the identified SQ or TQ site on each protein and supporting the quality of the peptide sequence identifications.

Functional analysis. Kinases may recognize many proteins, only a subset of which are significant to the kinase regulatory network. To examine this, we randomly chose a group of 37 substrates not previously implicated in the DDR to investigate genetically for roles in the DDR. We assayed cells depleted for these proteins with small interfering RNA (siRNA) for six basic phenotypes: the ability to prevent the spontaneous generation of DSBs, the ability to phosphorylate histone H2AX (H2A histone family member X) after IR, the ability to repair DSBs, activation of the G_2-M checkpoint, activation of the intra–S phase checkpoint, and the functionality of homologous recombination (HR).

In osteosarcoma U2OS cells, the γH2AX signal is low in the absence of IR, but rises rapidly and reaches maximal levels within 0.5 to 1 hour after 10 Gy IR. Thereafter, it decays rapidly as damage is being repaired and falls below 30% of peak levels by 6 hours after IR. We examined the effects of siRNA-mediated knockdown of candidate genes on formation of IR-induced γH2AX at these times in U2OS cells by Western blotting (Fig. 3A) to expose the potential roles of a gene in the maintenance of DNA integrity in the absence of damage or in the generation of γH2AX signal in response to damage or in DNA repair. siRNAs against many of the candidate genes altered the γH2AX signal compared with control siRNA (Fig. 3B and fig. S4). Inhibition of multiple genes from the list also showed functional defects in other assays (tables S4 to S6).

In summary, siRNAs against 35 of the 37 genes (94.6%) scored in at least one of the four assays, and more than half of the genes (22 genes) scored in two or more assays. siRNAs against CSTF2 (cleavage stimulation factor 2), DCK (deoxycytidine kinase), KIAA1160, NASP (nuclear autoantigenic sperm protein), RBM10 (RNA binding motif protein 10), SMARCAD1 (SWI/SNF-related, matrix-associated actin-dependent regulator of chromatin, subfamily a, containing DEAD/H-box 1), SRCAP (Snf2-related CBP activator protein), TPR (translocated promoter region), and USP34 (ubiquitin-specific peptidase 34) scored in three categories. LATS1 (large tumor suppressor homolog 1) scored in all four (Fig. 3C), as well as KIAA1794 (not shown), which we have found to encode FANCI, a novel component of the Fanconi anemia (FA) pathway (*16*). During the course of this study, involvement of RENT (regulator of nonsense transcripts) and FOXO1 (forkhead box 1) in the DDR pathway was shown (*17*, *18*), consistent with our observations. Thus, we concluded that our gene list is highly enriched with genes that regulate the DNA damage response or DNA repair.

Bioinformatic analysis of phosphorylation targets. The identified proteins were annotated in the gene ontology format. Of the 700 identified proteins, 421 were annotated with a biological process by the PANTHER program (Fig. 4A). Among these, 202 (48%) were assigned in the nucleic acid metabolism category that includes DNA replication, DNA repair, and other categories that involve nucleic acids. Further subdivision of these 202 revealed that 46 function in DNA replication, repair, or recombination and 101 function in mRNA transcription (Fig. 4B).

Another measure of the significance of certain functional categories among these phosphorylation targets is their enrichment relative to the total numbers in their respective categories. The DNA replication, recombination, and repair category showed a highly significant enrichment. Enrichments were also observed for proteins in the cell cycle, gene expression, and cell signaling categories (Fig. 4C). A surprising category with enrichment was the RNA posttranscriptional modification group that includes splicing factors and other RNA binding proteins potentially im-

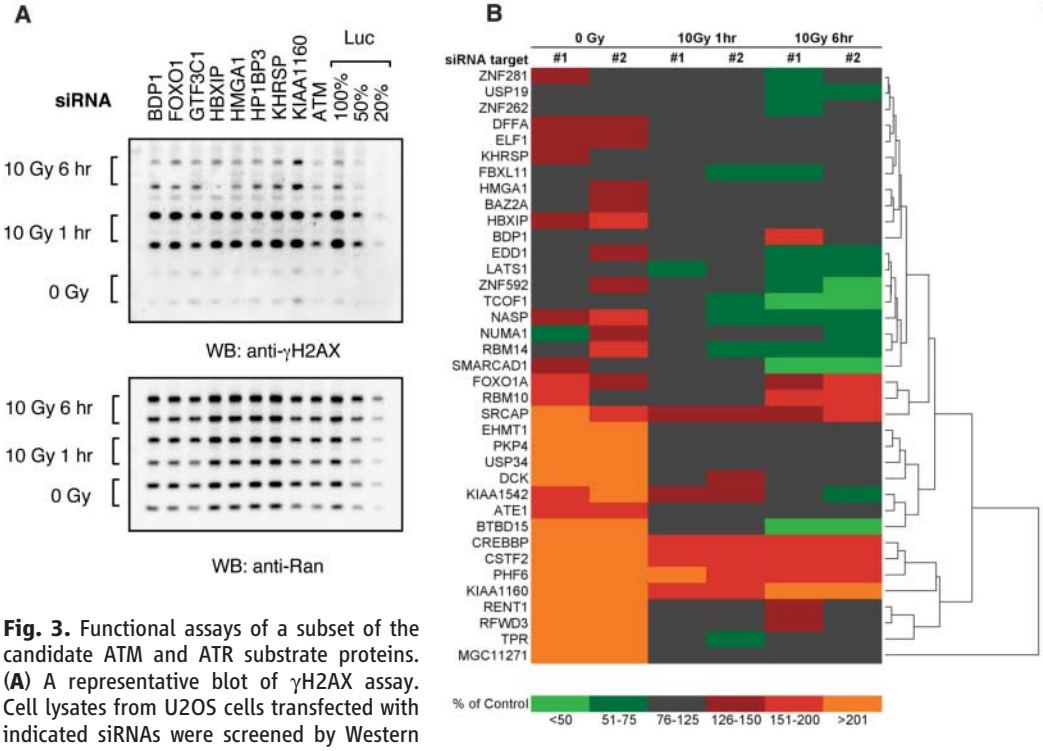

C

HR	G2/M	Intra-S	γH2AX
ATE1	ATE1	ATE1	ATE1
BAZ2A	BAZ2A	BAZ2A	BAZ2A
BDP1	BDP1	BDP1	BDP1
BTBD15	BTBD15	BTBD15	BTBD15
CREBBP	CREBBP	CREBBP	CREBBP
CSTF2	CSTF2	CSTF2	CSTF2
DCK	DCK	DCK	DCK
DFFA	DFFA	DFFA	DFFA
EDD1	EDD1	EDD1	EDD1
EHMT1	EHMT1	EHMT1	EHMT1
ELF	ELF	ELF	ELF
FBXL11	FBXL11	FBXL11	FBXL11
FOXO1A	FOXO1A	FOXO1A	FOXO1A
HBXIP	HBXIP	HBXIP	HBXIP
HMGA1	HMGA1	HMGA1	HMGA1
KHRSP	KHRSP	KHRSP	KHRSP
KIAA1160	KIAA1160	KIAA1160	KIAA1160
KIAA1542	KIAA1542	KIAA1542	KIAA1542
LATS1	LATS1	LATS1	LATS1
MGC11271	MGC11271	MGC11271	MGC11271
NASP	NASP	NASP	NASP
NUMA1	NUMA1	NUMA1	NUMA1
PHF6	PHF6	PHF6	PHF6
PKP4	PKP4	PKP4	PKP4
RBM10	RBM10	RBM10	RBM10
RBM14	RBM14	RBM14	RBM14
RENT	RENT1	RENT	RENT1
RFWD3	RFWD3	RFWD3	RFWD3
SMARCAD1	SMARCAD1	SMARCAD1	SMARCAD1
SRCAP	SRCAP	SRCAP	SRCAP
TCOF1	TCOF1	TCOF1	TCOF1
TPR	TPR	TPR	TPR
USP19	USP19	USP19	USP19
USP34	USP34	USP34	USP34
ZNF262	ZNF262	ZNF262	ZNF262
ZNF281	ZNF281	ZNF281	ZNF281
ZNF592	ZNF592	ZNF592	ZNF592

Fig. 3. Functional assays of a subset of the candidate ATM and ATR substrate proteins. (**A**) A representative blot of γH2AX assay. Cell lysates from U2OS cells transfected with indicated siRNAs were screened by Western blot using antibodies to γH2AX (top) and Ran as the loading control (bottom). (**B**) The normalized γH2AX signal from cells transfected with siRNAs was measured as a percentage of that with siRNA against luciferase and represented by one-dimensional hierarchical clustering. (**C**) Summary of the assay results: homologous recombination assay (HR), G_2-M checkpoint assay (G2/M), intra–S phase checkpoint–radio-resistant DNA synthesis assay (Intra-S), and γH2AX assay (γH2AX). Proteins scored in each assay are marked in red. Abbreviations not mentioned in text are spelled out in table S1. Detailed results of each assay are provided as tables S4 to S6.

plicated in RNA modification or translational control.

Discussion

In this study, we have identified more than 900 phosphorylation sites containing a consensus ATM and ATR phosphorylation motif in 700 proteins that are inducibly phosphorylated in response to IR. The extent of phosphorylation we observed was unanticipated. For example, among the mediator class of proteins, including BRCA1, 53BP1, and TopBP1, a total of 33 regulated sites were identified, 15 in 53BP1 alone. Of these 33, only 6 had been previously identified, and these are considered highly studied substrates. The quality of the identifications is supported by the fact that many sites were found multiple times and in different forms, such as a partial tryptic peptide or a peptide containing an oxidized methionine or in IPs with different antibodies, from cells with different types of DNA damage (table S7), or from different organisms (table S2). Furthermore, we chose a stringent cutoff for identification to reduce the frequency of false calls. Independent analysis of phosphorylation of randomly chosen genes from the list demonstrated that a high percentage could be verified.

Protein kinases are switches that coordinate entire programs dedicated to accomplishing the goals of a given signal transduction pathway. In this study, we discovered that damage-activated kinases do not simply contact key individual proteins in a process, but instead phosphorylate multiple components of particular pathways. Many of the proteins identified cluster into modules of previously known interacting proteins.

Interacting modules involved in DNA replication. Multiple modules involved in DNA replication were identified, such as an Orc module with Orc3 and Orc6 (Fig. 5A); an MCM (minichromosome maintenance protein) module including MCM2, MCM3, MCM6, MCM7, and MCM10; and DBF4, an activating subunit of the Cdc7 kinase needed for initiation of DNA replication (Fig. 5B). In addition, several components of the replication machinery emerged, including an RFC clamp–loader module (Fig. 5C) with RFC1 and RFC3 (replication factors C1 and C3) and a DNA polymerase module that includes the catalytic subunit of DNA polymerase epsilon (POLE), its interacting protein POLE4, and two translesion polymerases PolL and PolQ (Fig. 5D). Furthermore, both components of the Timeless-Tipin complex involved in fork stability were identified along with Claspin, with which they interact (*19*) (fig. S5F). These modules themselves interact in a larger network dedicated to DNA replication (fig. S6). Of these, only MCM2 and MCM3 were previously known ATM substrates (*10*, *20*). These findings indicate that the connections from the DDR to DNA replication are more complex than previously anticipated. As DNA damage signaling is known to control initiation of origins, as well as fork stability, the intra–S phase checkpoint, and restarting of forks after damage, it is likely that these new components take part in executing those processes.

Interacting modules involved in DNA repair. Multiple modules identified in this analysis function in control of DNA repair. A mismatch repair module contained mutS homolog genes MSH2, MSH3, and MSH6, as well as exonuclese 1 (EXO1) (Fig. 5E). This pathway is generally thought to act to repair mismatches during DNA replication.

An excision repair module included XPA and XPC (xeroderma pigmentosum complementation groups A and C); RPA1 (replication protein A1); ERCC6 (excision repair cross-complementing 6, also known as CSB, Cockayne syndrome group B); and components of transcription factor TFIIH (Fig. 5F). Other than RPA1, which participates in many repair pathways, this pathway had not been previously linked to DNA damage signaling.

We also found a module containing the Fanconi anemia (FA) pathway, which includes FANCD2, FANCA, and the newly discovered FANCI gene, which was identified through this screen (Fig. 5G). This module also contains BRCA2 and PALB2 (partner and localizer of BRCA2, FLJ21816), a BRCA2-binding protein involved in the FA pathway (*21*). A total of 12 regulated SQ or TQ phosphorylation sites were present in this module. Related to the FA

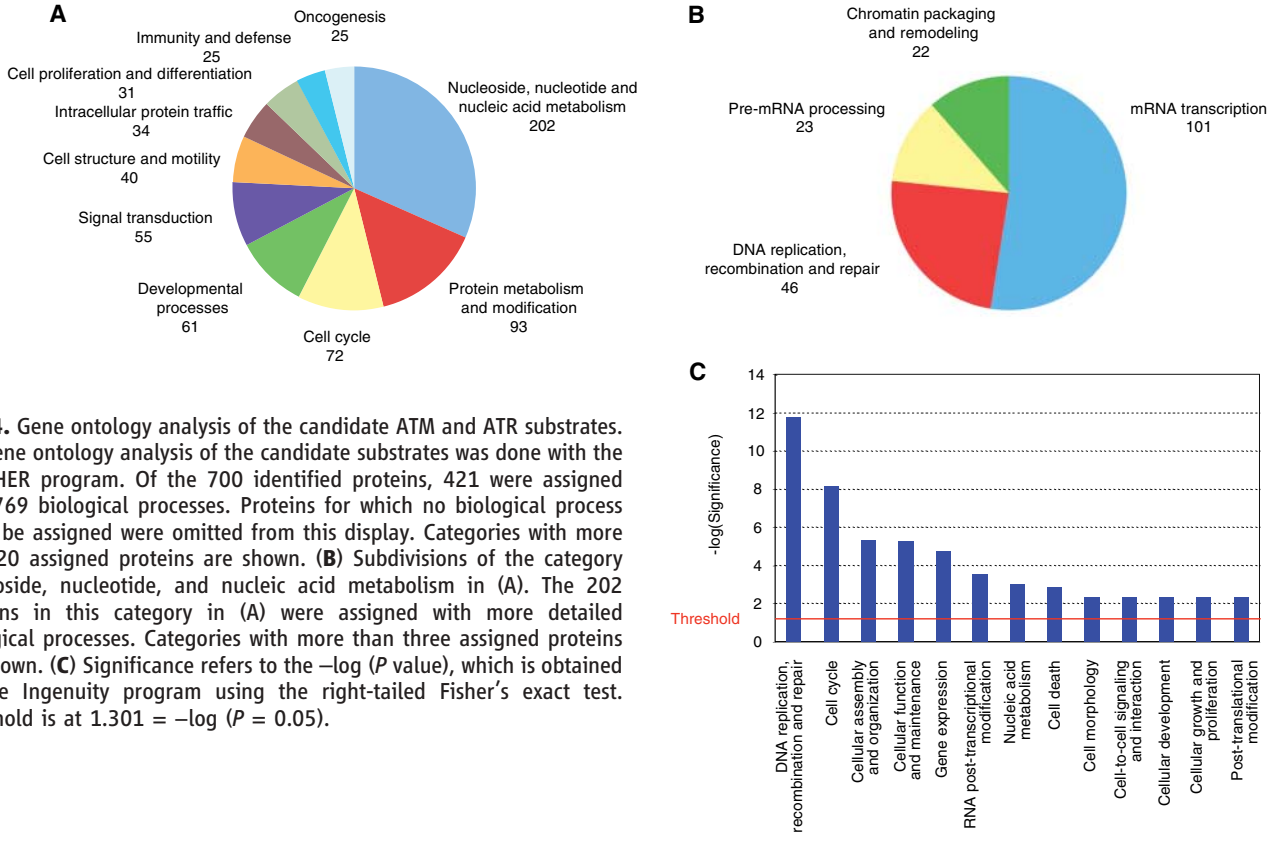

Fig. 4. Gene ontology analysis of the candidate ATM and ATR substrates. (**A**) Gene ontology analysis of the candidate substrates was done with the PANTHER program. Of the 700 identified proteins, 421 were assigned with 769 biological processes. Proteins for which no biological process could be assigned were omitted from this display. Categories with more than 20 assigned proteins are shown. (**B**) Subdivisions of the category nucleoside, nucleotide, and nucleic acid metabolism in (A). The 202 proteins in this category in (A) were assigned with more detailed biological processes. Categories with more than three assigned proteins are shown. (**C**) Significance refers to the –log (*P* value), which is obtained by the Ingenuity program using the right-tailed Fisher's exact test. Threshold is at 1.301 = –log (*P* = 0.05).

pathway is an extensive HR module including RAD50, RAD52, RAD51AP, RAD54, XRCC2, XRCC3, BRCA2, and PALB2, as well as RUVBL2 and TOP3 (not shown), representing essentially every step in the recombination process (Fig. 5H). Of the proteins in these two modules, only FANCD2 was previously known to be phosphorylated in response to DNA damage. These extensive contacts indicate that the processes of cross-link repair and HR are likely to be heavily regulated by the ATM and ATR pathway (Fig. 5, G and H).

An additional module implicated in DNA damage responses was the COP9 signalosome CSN, in which three subunits underwent phosphorylation: CSN1 (GPS1), COP3, and COP7A (Fig. 5I). This complex is involved in the SCF (Skp1–Cullin–F-box protein) pathway, where it participates in a neddylation-deneddylation cycle important in SCF E3 ligase function and alters its association with CSA (Cockayne syndrome type A) and DDB2 (damage-specific DNA binding protein 2), two DCAF (DDB1- and Cul4-associated factors) proteins in Cul4 ligases (*22*). In response to DNA damage, the CSN complex rearranges from DDB2-Cul4 complexes to CSA-Cul4 complexes.

New cell cycle modules. One cell cycle module found comprises cyclin E and two negative regulators of cyclin E: the F-box protein FBW7, which targets cyclin E for ubiquitination and destruction, and the cyclin-dependent kinase (Cdk) inhibitor $p27^{Kip1}$, which binds to cyclin E–Cdk2 complexes and inhibits their activity (Fig. 5J). In addition, the CIZ1 (Cip1 interacting Zn-finger protein), which negatively regulates the Cdk inhibitor $p21^{Cip1}$ and promotes DNA synthesis, is phosphorylated. This suggests that, in addition to causing cell cycle arrest through the Chk2-p53-$p21^{Cip1}$ pathway (*23*), DNA damage might also directly regulate the activity of cyclin E through additional inhibitors and proteolysis to promote cell cycle arrest.

We identified four components of the spindle checkpoint, Bub1, Mad1, Sgo1, and Mad2BP (Mad2 binding protein; also known as $p31^{COMET}$) (Fig. 5K). Bub1, Mad1, and Sgo1 promote mitotic arrest by maintaining Mad2-Cdc20 complex formation in response to unoccupied kinetochores, whereas Mad2BP opposes Mad2 function. In budding yeast, the spindle checkpoint and DNA damage checkpoint regulate a common protein, Pds1, and both checkpoints help to restrain cell cycle arrest in response to DNA damage, but no direct connections had been previously identified in mammals. The spindle checkpoint controls anaphase-promoting

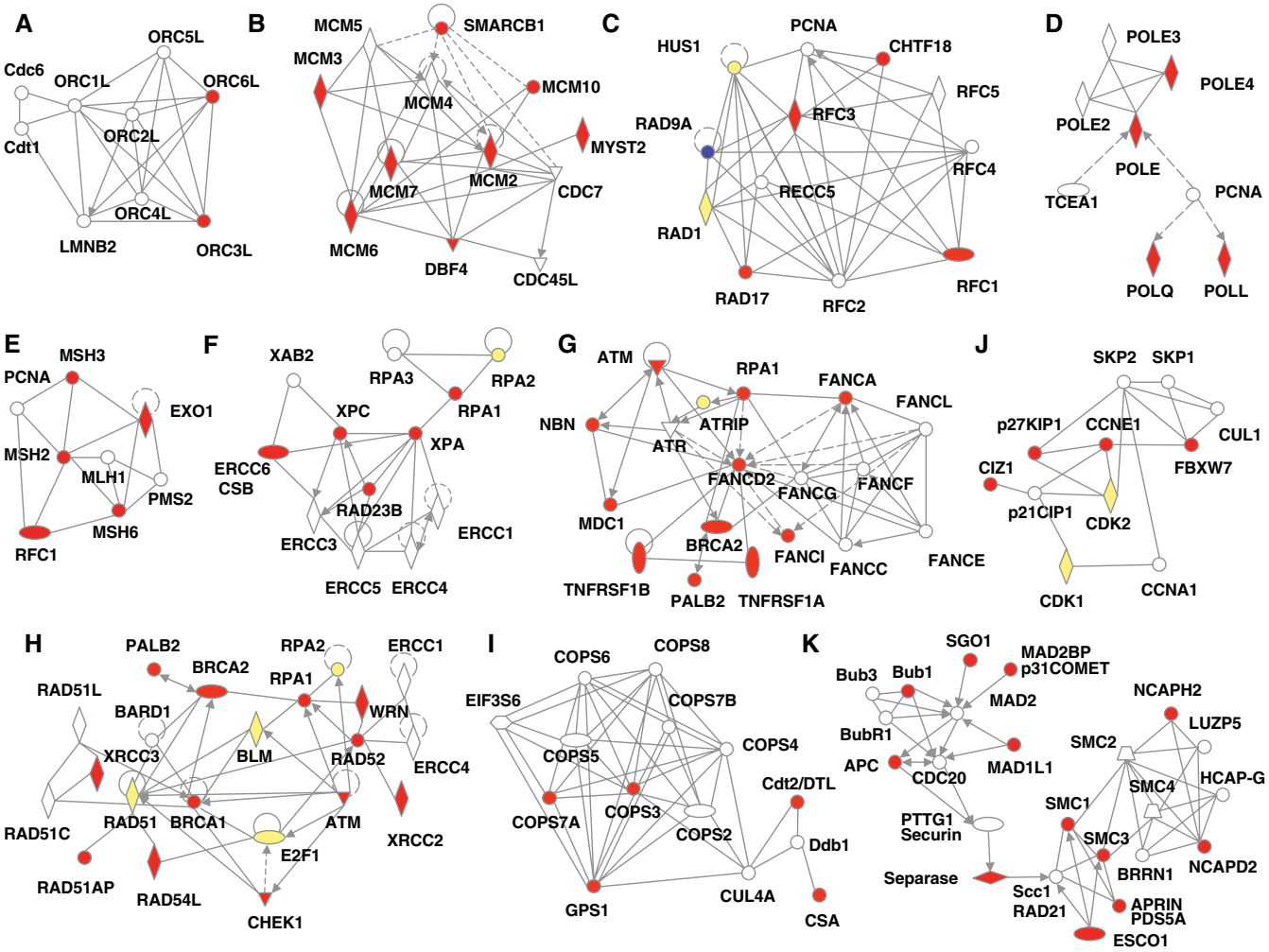

Fig. 5. Network modeling. Modules identified by using the Ingenuity program are (**A**) Orc module, (**B**) MCM module, (**C**) RFC module, (**D**) DNA polymerase module, (**E**) MSH module, (**F**) XP module, (**G**) FANC module, (**H**) BRCA1 module, (**I**) COP9 module, (**J**) cyclin E module, and (**K**) spindle checkpoint module. In each module, a solid line indicates direct interaction; a dashed line indicates indirect interaction; a line without arrowhead indicates binding; an arrow from protein A to protein B indicates A acts on B. Node shapes are indicative: triangle, kinase; diamond, enzyme; hexagon, translation regulator; trapezoid, transporter; oval (horizontal), transcription regulator; oval (vertical), transmembrane receptor. Proteins identified in this screen are marked in red and proteins known to be phosphorylated after IR but not identified in this screen are marked in yellow. Rad9 [marked in blue in (C)] was identified in peptide IP from cells damaged with ultraviolet light (table S7).

complex (APC) activation, which ultimately controls Separase activation, a protease that catalyzes dissolution of sister chromatid cohesion and anaphase entry. Both Cdc26, an APC subunit, and Separase were phosphorylated in response to IR (Fig. 5K). Components of the cohesion regulatory machinery were detected in our screen, including the cohesins SMC1 and SMC3 and the ESCO1 (establishment of cohesion 1 homolog 1) complex required for loading cohesins during S phase. Furthermore, APRIN, the human homolog of the *Saccharomyces cerevisiae* cohesion protein Pds5, was phosphorylated. An additional module that interacts with cohesin involves the Condensin II chromosome-condensation complex, including the substrates NCAPD2 and NCAPH2 (non-SMC condensing I complex subunits D2 and H2), which are both required for proper cohesion between sisters. Of these, only SMC1 was a known ATM substrate (*24*, *25*). These findings suggest that the DDR pathway displays manifold interfaces with other pathways previously implicated in cell cycle control.

Signaling pathways that interface with the DNA damage pathway. Various signaling pathways were also implicated in the DDR through this study. Enrichment was found for proteins in the insulin–IGF-1 (insulin-like growth factor)–PI3K (phosphatidylinositol 3-kinase)–AKT pathway, including the adaptor molecule IRS2 (insulin receptor substrate 2), the kinase AKT3, two regulators of AKT, HSP90 (heat shock protein 90), and PP2A (protein phosphatase 2A), and several downstream effectors of AKT. Examples of these downstream effectors are a transcription factor, FOXO1, and components in the proteins translation control pathway, TSC1 (tuberous sclerosis 1), 4E-BP1 (eIF4E binding protein 1), and p70S6K (ribosomal protein S6 kinase) (Fig. 6). Indeed, S^{111} of 4E-BP1, which we identified as a DNA damage–regulated site, is phosphorylated by ATM in response to insulin (*26*). The enriched set of contacts between the DDR and the insulin signaling pathway suggests that the DDR might induce a survival signal through the activation of AKT. Our study indicates that the DDR is likely to intersect the insulin–IGF-1–PI3K–AKT pathway at many points. In support of this idea, mice lacking the nucleotide excision repair protein ERCC1 show both accelerated aging (due to constitutive DNA damage) and severe growth retardation (due to suppression of the growth hormone–IGF-1 axes) (*27*). Although DNA damage could affect insulin and IGF-1 signaling in vivo through indirect effects such as the depletion of stem cells in the liver and the pancreas, it is also possible that persistent repetitive DNA damage alters cellular insulin–IGF-1 signaling and contributes to diabetes and other age-associated metabolic disorders.

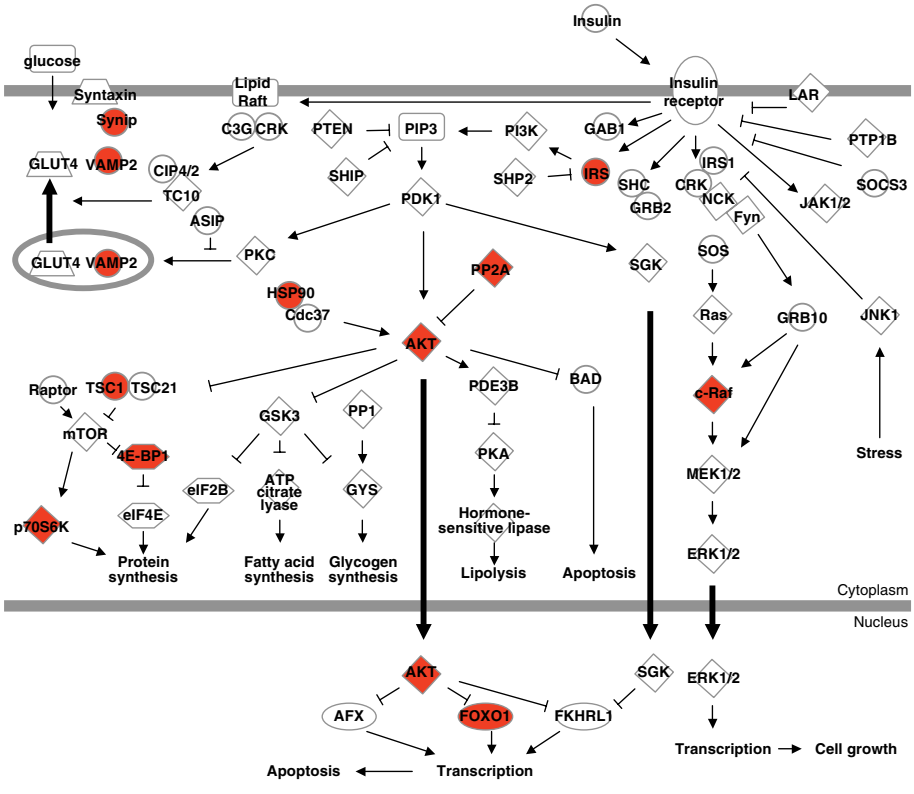

Fig. 6. Possible involvement of the AKT-insulin pathway in the DDR. Node shapes are indicative: rectangle, cytokine; diamond, enzyme; oval (horizontal), transcription regulator; oval (vertical), transmembrane receptor; trapezoid, transporter; hexagon, translation regulator. Proteins identified in this screen were marked in red.

Many other pathways not mentioned here appear to have multiple connections to the DNA damage pathway. At this point it is not clear whether these are all substrates of ATM and ATR or possibly other kinases activated by IR. In addition to DSBs, IR causes oxidative stress and ssDNA breaks. How these events are sensed and whether kinases participate in signaling detection of these events is not known. Any kinase activated by IR could recognize a site that happens to have a Q adjacent to S or T, potentially marking it for identification by our method. In fact, only 70% of our substrates appear to be regulated by ATM (table S8, A and B). Others could be ATR and DNA-PK substrates. Alternatively, it is possible that other phosphatidylinositol 3-kinase–related kinase (PIKK) members respond to secondary stresses generated by this treatment. In this vein, we identified a module around the nonsense-mediated decay pathway containing the PIKK SMG1 and RENT as regulated substrates (fig. S5C). SMG1 can phosphorylate RENT on SQ sites (*28*). This pathway has been previously implicated in the response to IR. It is not clear if it is downstream of ATM, or if SMG1 senses damage to DNA or possibly to RNA.

We also found a large number of proteins involved in chromatin modification and transcription, including subunits of multiple RNA polymerases and many proteins involved in splicing and RNA metabolism (fig. S5, A to C and E). This points to a broad cellular transcriptional, posttranscriptional, and chromatin response that had only been hinted at in previous studies.

It is likely that we have identified the majority of abundant proteins inducibly phosphorylated on SQ or TQ sites after DNA damage. The DNA damage phosphorylation database is a rich resource of information that can be used in multiple ways. In one instance, we identified a novel FA gene by phenotypic analysis (*16*). In another case, we used the BRCT repeats of BRCA1 to pull down tryptic peptides and proteins. By looking for proteins in common between those purifications and this database, we identified two novel BRCA1-binding proteins (*29*). Combining these data and other data sets should allow important damage-response proteins to be identified and new pathways to be explored.

The results of this study illustrate the extraordinarily broad landscape of the DDR, which extends far beyond what was anticipated from previous studies. The large number of functional modules discovered here and the multiple connections to each suggest that the DDR profoundly alters cellular physiology. The elucidation of these newfound connections and the roles played by the many proteins newly implicated in the damage response should provide a solid foundation for a systems biology understanding of the cellular response to DNA damage and replication stress in the future.

References and Notes

1. B. B. Zhou, S. J. Elledge, *Nature* **408**, 433 (2000).
2. M. B. Kastan, J. Bartek, *Nature* **432**, 316 (2004).
3. Y. Shiloh, *Trends Biochem. Sci.* **31**, 402 (2006).
4. J. Ptacek *et al.*, *Nature* **438**, 679 (2005).
5. N. Dephoure, R. W. Howson, J. D. Blethrow, K. M. Shokat, E. K. O'Shea, *Proc. Natl. Acad. Sci. U.S.A.* **102**, 17940 (2005).
6. A. R. Salomon *et al.*, *Proc. Natl. Acad. Sci. U.S.A.* **100**, 443 (2003).
7. J. Rush *et al.*, *Nat. Biotechnol.* **23**, 94 (2005).
8. S. T. Kim, D. S. Lim, C. E. Canman, M. B. Kastan, *J. Biol. Chem.* **274**, 37538 (1999).
9. T. O'Neill *et al.*, *J. Biol. Chem.* **275**, 22719 (2000).
10. D. Cortez, G. Glick, S. J. Elledge, *Proc. Natl. Acad. Sci. U.S.A.* **101**, 10078 (2004).
11. Y. Ziv *et al.*, *Nat. Cell Biol.* **8**, 870 (2006).
12. M. Mann, *Nat. Rev. Mol. Cell Biol.* **7**, 952 (2006).
13. S. V. Kozlov *et al.*, *EMBO J.* **25**, 3504 (2006).
14. G. P. Ho, S. Margossian, T. Taniguchi, A. D. D'Andrea, *Mol. Cell. Biol.* **26**, 7005 (2006).
15. K. C. Thome *et al.*, *J. Biol. Chem.* **275**, 35233 (2000).
16. A. Smogorzewska *et al.*, *Cell* **129**, 289 (2007).
17. C. M. Azzalin, J. Lingner, *Curr. Biol.* **16**, 433 (2006).
18. H. Huang, K. M. Regan, Z. Lou, J. Chen, D. J. Tindall, *Science* **314**, 294 (2006).
19. N. Yoshizawa-Sugata, H. Masai, *J. Biol. Chem.* **282**, 2729 (2006).
20. H. Y. Yoo, A. Shevchenko, W. G. Dunphy, *J. Biol. Chem.* **279**, 53353 (2004).
21. B. Xia *et al.*, *Mol. Cell* **22**, 719 (2006).
22. R. Groisman *et al.*, *Cell* **113**, 357 (2003).
23. A. Hirao *et al.*, *Science* **287**, 1824 (2000).
24. P. T. Yazdi *et al.*, *Genes Dev.* **16**, 571 (2002).
25. S. T. Kim, B. Xu, M. B. Kastan, *Genes Dev.* **16**, 560 (2002).
26. D. Q. Yang, M. B. Kastan, *Nat. Cell Biol.* **2**, 893 (2000).
27. L. J. Niedernhofer *et al.*, *Nature* **444**, 1038 (2006).
28. K. M. Brumbaugh *et al.*, *Mol. Cell* **14**, 585 (2004).
29. B. Wang *et al.*, *Science* **316**, 1194 (2007).
30. Single-letter abbreviations for the amino acid residues are as follows: A, Ala; C, Cys; D, Asp; E, Glu; F, Phe; G, Gly; H, His; I, Ile; K, Lys; L, Leu; M, Met; N, Asn; P, Pro; Q, Gln; R, Arg; S, Ser; T, Thr; V, Val; W, Trp; and Y, Tyr.
31. B. A. Ballif, Z. Cao, D. Schwartz, K. L. Carraway III, S. P. Gygi, *J. Proteome Res.* **5**, 2372 (2006).
32. B. DeLaBarre, A. T. Brunger, *Nat. Struct. Biol.* **10**, 856 (2003).

33. We thank T. de Lange, A. D'Andrea, A. Carr, K. Nakanishi, M. Jasin, H. Takai, F. Graham, D. Zhang, D. Chou, B. Wang, M. Naylor, J.-M. Li, D. Lee, C. Zhou, and C. Cotta-Ramusino for reagents and advice; J. Qin for antibodies and sharing unpublished data; K. Matsuoka for helping with preparation of figures; and P. Park and Q. Xu for help with the bioinformatic analysis. A.S. is supported by T32CA09216 to the Pathology Department at the Massachusetts General Hospital. K.E.H. is a Leukemia and Lymphoma Society Special Fellow. This work was supported by grants from NIH, including National Institute of Allergy and Infectious Diseases 1U19A1067751 (S.J.E.), and Department of Defense (S.J.E. and S.P.G.) and by the A-T (Ataxia-Telangiectasia) Medical Research Foundation, the A-T Children's Project, the Israel Science Foundation, the A-T Medical Research Trust, the Israel-Germany Joint Program on Cancer Research, the German Cancer Center DKFZ (Deutsches Krebsforschungszentrum), and the A-T Ease Foundation (Y.S.). S.J.E. is an investigator with the Howard Hughes Medical Institute.

Supporting Online Material

www.sciencemag.org/cgi/content/full/316/5828/1160/DC1
Materials and Methods
Figs. S1 to S7
Tables S1 to S10
References

24 January 2007; accepted 6 April 2007
10.1126/science.1140321

REPORTS

Missing Mass in Collisional Debris from Galaxies

Frédéric Bournaud,[1]* Pierre-Alain Duc,[1] Elias Brinks,[2] Médéric Boquien,[1] Philippe Amram,[3] Ute Lisenfeld,[4,5] Bärbel S. Koribalski,[6] Fabian Walter,[7] Vassilis Charmandaris[8,9,10]

Recycled dwarf galaxies can form in the collisional debris of massive galaxies. Theoretical models predict that, contrary to classical galaxies, these recycled galaxies should be free of nonbaryonic dark matter. By analyzing the observed gas kinematics of such recycled galaxies with the help of a numerical model, we demonstrate that they do contain a massive dark component amounting to about twice the visible matter. Staying within the standard cosmological framework, this result most likely indicates the presence of large amounts of unseen, presumably cold, molecular gas. This additional mass should be present in the disks of their progenitor spiral galaxies, accounting for a substantial part of the so-called missing baryons.

When galaxies collide, gravitational forces cause the expulsion of material from their disks into the intergalactic medium. In this debris, dense self-gravitating structures form. Because they can reach masses typical of those of dwarf galaxies and they show ordered rotation and active star formation (*1*–*8*), they deserve to be considered galaxies in their own right, albeit "recycled" ones. Whether these recycled dwarf galaxies contain dark matter can put strong constraints on the nature and distribution of this enigmatic constituent of the Universe. Indeed, standard theory (*9*–*11*) predicts that they differ from classical galaxies by being nearly free of nonbaryonic dark matter (*5*, *7*, *12*). According to the widely accepted ΛCDM (cold dark matter with cosmological constant) model (*13*), the matter density of the Universe is dominated by nonbaryonic dark matter. This matter is expected to surround galaxies in the form of large halos supported by random motions (*9*). Recycled galaxies are expected to have little, if any, dark matter of this type, because only material from rotating disks is involved in the galactic recycling process. In addition to nonbaryonic dark matter, part of the baryonic component is "dark" as well [i.e., it is known to have existed in the early Universe (*14*), but it is hard or impossible to detect locally today]. It has been speculated to be cold gas (*15*, *16*) but is most widely thought to reside in a diffuse warm-hot intergalactic medium (WHIM) that surrounds galaxies (*10*, *11*) and that cannot be substantially accumulated in collisional debris. Hence, recycled dwarf galaxies are predicted by conventional views to be mostly free of both baryonic and nonbaryonic dark matter. We put these views to the test, measuring the mass of three galaxies formed in the collisional debris around galaxy NGC5291 (*17*, *18*).

The galaxy NGC5291 is surrounded by a large, gas-rich ring of collisional debris (*17*). In several places, gas has gathered into self-gravitating, rotating dwarf galaxies where new stars form (Fig. 1). We studied the kinematics of atomic hydrogen in the ring through its 21-cm emission line, using the National Radio Astronomy Observatory (*19*) Very Large Array (VLA) interferometer in a high-resolution configuration. We estimated the mass actually present in the dwarf galaxies and compared this to their visible mass (*6*, *18*, *20*, *21*). We used *N*-body simulations that model the gravitational dynamics of stars, gas, and dark matter halos, with 1 million particles for each component. The model also accounts for energy dissipation in the interstellar gas, and the onset of star formation (*22*), reproducing both the global morphology of the NGC5291 system and the formation of recycled dwarf galaxies in it. These simulations enable us to date the formation of the system and to study its three-dimensional morphology. According to our model (*23*), the ring formed during a galaxy collision 360 million years ago and is seen inclined by 45° from the line of sight (Fig. 1 and figs. S1 and S2).

[1]Laboratoire Astrophysique des Interactions Multi-Echelles, Commissariat à l'Energie Atomique (CEA) Direction des Sciences de la Matière–CNRS–Université Paris Diderot, Laboratoire de recherches sur les lois fondamentales de l'Univers (Dapnia)/Service d'Astrophysique, CEA/Saclay, F-91191 Gif-sur-Yvette Cedex, France. [2]Centre for Astrophysics Research, University of Hertfordshire, College Lane, Hatfield, AL10 9AB, UK. [3]Observatoire Astronomique Marseille-Provence, Laboratoire d'Astrophysique de Marseille UMR 6110, 2 place Le Verrier, F-13248 Marseille Cedex 4, France. [4]Departamento Física Teórica y del Cosmos, Universidad de Granada, Spain. [5]Instituto de Astrofísica de Andalucía (CSIC), Post Office Box 3004, 18080 Granada, Spain. [6]Commonwealth Scientific and Industrial Research Organisation (CSIRD), Australia Telescope National Facility (ATNF), Post Office Box 76, Epping NSW 1710, Australia. [7]Max Planck Institut für Astronomie, Königstuhl 17, 69117 Heidelberg, Germany. [8]Department of Physics, University of Crete, GR-71003 Heraklion, Greece. [9]Foundation for Research and Technology (IESL), Hellas, GR-71110, Heraklion, Greece. [10]Observatoire de Paris, F-75014, Paris, France.

*To whom correspondence should be addressed. E-mail: frederic.bournaud@cea.fr